A Novel Sensing Method to Detect Tissue Boundaries during Robotic Needle Insertion Based on Laser Doppler Flowmetry

Vani Virdyawan[1], Orsina Dessi [1] and Ferdinando Rodriguez y Baena[1]

***Abstract*—This study investigates the use of Laser Doppler Flowmetry (LDF) as a method to detect tissue transitions during robotic needle insertions. Insertions were performed in gelatin tissue phantoms with different optical and mechanical properties and into *ex-vivo* sheep brain. The effect of changing the optical properties of gelatin tissue phantoms was first investigated and it was shown that using gelatin concentration to modify the stiffness of samples was suitable. Needle insertion experiments were conducted into both one-layer and two-layer gelatin phantoms. In both cases, three stages could be observed in the perfusion values: tissue loading, rupture and tissue cutting. These were correlated to force values measured from the tip of the needle during insertion. The insertions into *ex-vivo* sheep brain also clearly showed the time of rupture in both force and perfusion values, demonstrating that tissue puncture can be detected using an LDF sensor at the tip of a needle.**

***Index Terms*—Surgical Robotics: Steerable Catheters/Needles; Force and Tactile Sensing.**

I. INTRODUCTION

MINIMALLY invasive surgery (MIS) uses long, thin instruments, such as needles or catheters, to perform surgeries through small percutaneous incisions in order to minimize collateral damage. This makes percutaneous needle interventions particularly desirable in neurosurgery, where minimising damage to the surrounding brain matter is vital due to its delicate and complex nature [1]. The benefits of MIS to patients also include shorter hospitalization periods and reduced recovery times [2]. However, as the surgeon does not have a direct view of the operating area during MIS due to the minimal access, there is a need for image guidance to reach the target correctly. However, imaging modalities for brain surgery are limited: ultrasound, for example, cannot easily pass through the skull.

One method to differentiate between healthy, unhealthy and different types of brain tissue pivots on the use of mechanical properties [3]. For instance, white matter is on average 39% stiffer than grey matter, with average moduli of 1.859 $\pm$ 0.592 kPa and 1.389 $\pm$ 0.289 kPa, respectively [4]. In mice, meningiomas have been found to be stiffer than healthy mouse brain, with an elastic modulus 2-5 times higher [5]. For this reason, elastography can be used to detect tissue boundaries between tissues of different stiffness. Kennedy et. al. [6] deployed optical coherence elastography into a needle probe in order to use elastography in deeper tissue. However, the needle used in their study had a flat tip, which is not suitable for implementation into the clinical environment [7]. In the robotics field, robotic needle insertion has attracted attention [8], especially in the field of needle steering, due to its ability to rectify misalignment during insertion. Since some robotic steerable needles rely on tool tissue interaction (e.g. bevel-tip needles [9], and programmable bevel-tip needles (PBNs) [10]), several groups have studied the process of tissue puncture as part of the control. Force sensors are predominantly used to predict tissue punctures and the passing of the needle through different structures [11], [12], [13], for example in [13], where a needle with embedded fibre Bragg grating (FBG) was used for strain detection during membrane puncture. Detecting differences in tissue stiffness has also been investigated in [14]. They show that in the area in front of the needle, stiffer tissue has less tissue deformation compared to softer tissue.

In our previous work, the use of Laser Doppler Flowmetry (LDF) probes as forward-looking sensors to detect the presence of a vessel at the tip of a steerable needle was investigated [15]. The steerable needle itself is based on a programmable bevel-tip needle (PBN). In this work, the use of LDF as a method to detect tissue transitions is explored, in particular with soft needles such as programmable bevel-tip needles (PBNs). PBNs are specifically designed to access deep lesions inside the brain [16], and offer a multi-segment design with an interlocking mechanism that links adjacent segments to allow for axial sliding. Compared to the tissue boundary detection methods based on force sensing (e.g. in [12], [13]), one of the advantages of a forward-viewing sensor, such as an LDF probe, is that it does not require any change to the mechanical design of the needle. Due to the small size of the probe (e.g. 0.3 mm for LDF probe used in this work), it can be inserted directly in the working channel of a needle.

LDF measures the movement of scattering particles, so the perfusion value recorded, a function of speed and the scattering of particles, is dependent also on the movement of tissue. Tissue movements should therefore be avoided since they would result in high perfusion values [17]. Since LDF is

Manuscript received: September 10, 2019; Revised December 5, 2019; Accepted January 10, 2020.

This paper was recommended for publication by Editor Pietro Valdastri upon evaluation of the Associate Editor and Reviewers' comments. This work was supported by European Union's Horizon 2020 research and innovation programme under grant agreement 688279 (EDEN2020), and Imperial Confidence in Concepts - Joint Translational Fund funded by EPSRC Impact Acceleration Account and MRC Confidence in Concept Scheme.

[1]All of the authors are from the Mechatronics in Medicine Laboratory, Mechanical Engineering Department, Imperial College London, London, UK. *Corresponding author: Ferdinando Rodriguez y Baena* f.rodriguez@imperial.ac.uk

Digital Object Identifier (DOI): see top of this page.

traditionally used to measure blood perfusion, this work is, to the authors' knowledge, the first time that LDF measurements are used as a method to detect tissue boundaries and to detect tissues of different stiffness by embedding a sensor within a needle.

In previous work [18] it was shown that the perfusion value is constant during needle insertion with constant insertion speed. However, only one type of tissue phantom was investigated. Other studies have investigated the use of force sensors to detect tissue boundaries. Since tissue stiffness can be classified by tissue deformation, in this study it is hypothesized that during the insertion process, tissue movement will be able to be differentiated by a movement sensor, in this case using Laser Doppler Flowmetry. The outline of the paper is as follows: section II discusses the tissue phantom that was used. In section III, the effect of different optical and mechanical properties on perfusion values are investigated. The comparison between force and perfusion values during the insertion process is then discussed in section III. In this section, an experiment using a one-layer tissue phantom, followed by another with a two-layer phantom, and *ex-vivo* insertion in a sheep's brain are presented. Section IV discusses the finding. This paper is concluded with section V, where a number of future research avenues are highlighted.

II. Tissue Phantom Preparation

A. Materials and Method

Gelatin tissue phantoms were used to investigate the effect of different tissue stiffnesses and different optical properties on the LDF measurements: perfusion value and total light intensity. Lipids (e.g. milk and intralipid solutions), microspheres, and titanium dioxide (TiO_2) are commonly used to change the reduced scattering coefficient of a tissue phantom [19]. TiO_2 is suitable for gelatin based disposable tissue phantom due to its lower price compared to the microsphere [19]. In our previous work, the mechanical properties of gelatin as a function of gelatin weight to liquid (i.e. water) weight ratio were investigated in order to develop a tissue phantom that mimics the mechanical properties of human brain [20]. The use of TiO_2 does not change the gelatin to liquid weight ratio compared to adding lipids. To change the absorption coefficient of a tissue phantom, Indian ink, whole blood, and molecular dyes can be used [19]. Indian ink is easy to find and provides nearly flat absorption spectra. Therefore TiO_2 and Indian ink were chosen to modify the optical properties of the tissue phantoms.

Gelatin samples were mixed using a magnetic stirrer for at least 35 minutes and then stored in a fridge for >12 hours. Once they had returned to room temperature these samples were tested on an Instron universal testing machine at a rate of 4/min (50mm/s) [20]. To investigate the effect of adding TiO_2 and indian ink, two tissue phantoms with 4.5% w/w gelatin were compared. The first sample was made with 3 g/L TiO_2 [21] and 0.005% [22] volume/volume Indian ink to mimic the optical properties of grey matter (reduced scattering coefficient (μ_s') = 0.76 mm^{-1} and absorption coefficient (μ_a) = 0.028 mm^{-1}) [23]. The second sample used 14.35% TiO_2 to mimic the optical properties of white matter (μ_s' = 4.1 mm^{-1} and μ_a = 0.005 mm^{-1}) [23]. To check that different stiffnesses could still be achieved by changing gelatin concentration, the white matter phantoms were tested at three different gelatin concentrations (2.5%, 4.5%, and 6.5% w/w). A minimum of five compression tests were performed for each sample.

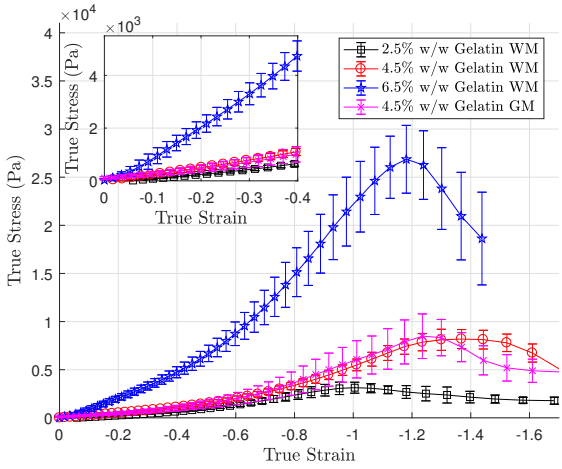

Fig. 1. Compression to failure test results for white matter phantom with different gelatin concentration (2.5%, 4.5%, and 6.5% w/w) and grey matter phantom with 4.5% gelatin concentration. WM: white matter phantom, GM: grey matter phantom

B. Results

Fig. 1 shows the stress-strain curve of the compression test. The mean and standard deviation of each sample are shown in Table I. The modulus of elasticity of each sample was calculated from their stress-strain curve up to -0.4 strain, as it is linear up to this point. Shapiro-Wilk tests were used to check the normality of the modulus of elasticity data of 4.5% w/w gelatin (p = 0.472 and p = 0.145 for white matter and grey matter phantom, respectively). The modulus of elasticity of 4.5% w/w gelatin grey matter and white matter phantoms were then compared using independent sample t-tests, which showed no statistically significant difference between the two (p = 0.180). The modulus of elasticity of different gelatin concentrations for white matter phantoms were then compared. As before, Shapiro-Wilk tests (α = 0.05) were used to check the normality of the data (p = 0.354, p = 0.875, and p = 0.423 for 2.5%, 4.5%, and 6.5% w/w gelatin, respectively). One-way Anova showed that there was a statistically significant difference between the modulus of elasticity of white matter phantoms ($F_{2,12}$ = 545.287, p $<$ 0.001). Post-hoc Tukey tests were used to show that $E_{2.5} \neq E_{4.5}$ (p = 0.034), $E_{2.5} \neq E_{6.5}$ (p $<$ 0.001), and $E_{4.5} \neq E_{6.5}$ (p $<$ 0.001), where $E_{2.5}$, $E_{4.5}$, and $E_{6.5}$ are the modulus elasticity of 2.5%, 4.5%, and 6.5% w/w gelatin, respectively. This showed that gelatin concentration could still be used to modify the stiffness of samples for needle insertion despite the changing optical properties.

III. Needle Insertion Experiments

Two types of needle insertions were performed, one into one-layer and another into two-layer gelatin. One-layer inser-

TABLE I
MEAN AND STANDARD DEVIATION (SD) OF THE ELASTIC MODULUS (E) OF THE TISSUE PHANTOMS

	Mean E (kPa)	SD E (kPa)
2.5% w/w WM	1.7	0.4
4.5% w/w WM	2.7	0.3
6.5% w/w WM	12.0	0.8
4.5% w/w GM	2.2	0.7

tions were used to investigate the effect of changing optical properties and tissue stiffness on the steady state perfusion value, and to investigate the relationship between force and perfusion value during puncture. Two layer insertions were used to investigate the effect of an abrupt change in tissue mechanical properties on perfusion value. After investigating the perfusion value during needle insertions into a soft tissue phantom, needle insertion experiments were performed into an *ex-vivo* sheep's brain.

A. Needle Insertion Materials and Methods

To investigate the effect of tissue stiffness on the perfusion values, phantoms with three different stiffnesses were made by changing the gelatin concentration (2.5%, 4.5%, and 6.5% weight/weight). The relationship between the optical properties of the tissue phantom and the perfusion values were also investigated. Therefore, each gelatin concentration was made with six different optical properties. Phantoms with the same set of optical properties were then grouped and labelled with #1, #2, #3, #4, #5, and #6. Table II shows the reduced scattering coefficient and the absorption coefficient of each group. To achieve these optical properties, the concentration of the TiO_2 and Indian ink in the sample were changed. 1 g/L of TiO_2 resulted in a reduced scattering coefficient (μ_s') of 0.22 mm^{-1} [21], while 0.005% Indian ink achieved an absorption coefficient (μ_a) of 0.025 mm^{-1} [22]. The absorption coefficient of gelatin without Indian ink is 0.005 mm^{-1}. The perfusion values of phantoms in groups #1, #2, #3, and #4 were compared to investigate the effect of absorption coefficient and tissue stiffness on the perfusion values, while the perfusion values of phantoms in group #3, #5, and #6 were compared to investigate the effect of tissue stiffness and reduced scattering coefficient to the perfusion values.

During insertion, the insertion force was recorded with a Nano43 (ATI Industrial Automation Inc., Apex, USA) force sensor using force along the z axis, which had a maximum force reading of 18 N and a resolution of 1/256 N. A commercial single channel Laser Doppler Flowmeter (OxyFlo™, Oxford Optronix Ltd., Abingdon, UK) with a bare-fibre type probe with a diameter of 0.3 mm (NX-BF/F, Oxford Optronix Ltd., Abingdon, UK) was used, embedded within the working channel of a 3D printed rigid needle with a diameter of 2.5 mm (see Fig. 2a). The rigid needle had the same outer dimension as the PBN used in [24]. The data logging of the LDF was performed using Labjack U3-HV (Labjack Corporation, Lakewood, USA). A MATLAB program was used to record all of the data. Both the force sensor and Labjack were in command-response mode to synchronise the data, at an average acquisition rate of 80 Hz. Automatic insertion was performed using a motorized translation stage (MTS50/M-Z8, Thorlabs Inc., New Jersey, USA). The insertion rig and the measurement set-up can be seen in Fig. 2. The insertion speed was set at 0.25 mm/s, which is half of the maximum insertion speed recommended to avoid hemorrhage during deep brain stimulation procedures [25]. In addition, for phantom #3, the effect of the insertion speed on perfusion value was also investigated. Three insertion speeds were investigated: 0.25, 0.5, and 0.75 mm/s.

It was shown in previous work that the needle insertion stages (tissue loading, rupture, and cutting) are repeated if the needle enters a different tissue layer [26]. This study further investigated whether using perfusion value to identify changes in tissue stiffness would work for a two layer tissue phantom. Two types of tissue transitions were used: hard-soft and soft-hard. Phantom #3 with 4.5% weight of gelatin was used for the soft tissue, and phantom #3 with 6.5% gelatin for the hard phantom. The insertion speed was set at 0.25 mm/s. For each sample, nine insertions were performed.

Insertion tests were then conducted in *ex-vivo* sheep's brain to ascertain the performance of the method in biological tissue. The brain was collected from a local butcher and the experiments were performed within 48 hours from the sheep being slaughtered. Tissue rupture was defined qualitatively as a drop in insertion force, as *in-situ* imaging as a ground truth (e.g. ultrasound) was not available.

B. Needle Insertion Results

Fig. 3a shows the corresponding force and perfusion value during needle insertion for phantom #3 with 2.5% w/w gelatin. The tissue loading, rupture, and tissue cutting insertion stages [26] can be seen in both the force profile, and in the changing perfusion values. Fig. 3b shows the box-plot of the steady state perfusion values during the tissue cutting stage with different gelatin concentration of the sample #1, #2, #3, and #4 (the same μ_s' but different μ_a values). Fig. 3c shows the box-plot of steady state perfusion values as a function of μ_a. Two-way ANOVA showed that there was a statistically significant difference in the perfusion value for different tissue stiffness ($p < 0.001$) and a statistically significant difference in the perfusion value for different μ_a. A post-hoc Tukey test also showed that the perfusion value in the 2.5% gelatin sample was higher compared to the perfusion value in both 4.5% (p=0.011) and 6.5% gelatin ($p < 0.001$). The absorption coefficient also has an effect on the perfusion value. The perfusion value in the phantom with μ_a = 0.005 mm^{-1} was higher compared to the perfusion in the phantom with μ_a = 0.03 mm^{-1} (p = 0.025) and μ_a = 0.05 mm^{-1} (p = 0.001). There was no statistically significant difference between perfusion values in

TABLE II
OPTICAL PROPERTIES OF THE TISSUE PHANTOMS FOR ONE-LAYER INSERTION

Phantom #	1	2	3	4	5	6
μ_s' (mm^{-1})	0.77	0.77	0.77	0.77	1.15	1.54
μ_a (mm^{-1})	0.005	0.03	0.05	0.08	0.05	0.05

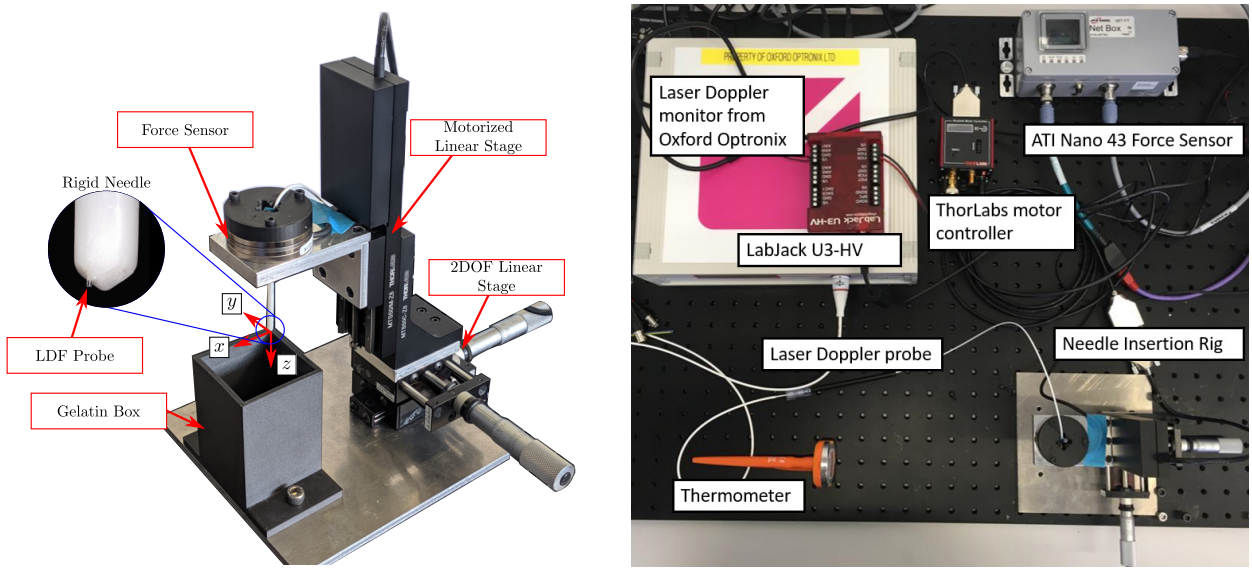

(a) (b)

Fig. 2. a) Needle insertion rig; b) experiment set-up for LDF and force measurement

the phantom with μ_a = 0.03 mm^{-1} and μ_a = 0.05 mm^{-1} (p = 0.657). Interestingly, the phantom with μ_a = 0.08 mm^{-1} had the highest perfusion value.

Fig. 3d shows a box-plot for the steady state perfusion values during the tissue cutting stage with different gelatin concentrations of samples #3, #5 and #6 (i.e. the same μ_a but different μ_s' values). Fig. 3e shows the box-plot of steady state perfusion values as a function of μ_s'. Two-way ANOVA showed that there was a statistically significant difference in the perfusion value for different tissue stiffnesses (p <0.001), but there was no statistically significant difference in the perfusion value for different μ_s' (p = 0.652). Similar to previous findings, a Post-hoc Tukey test also showed that the perfusion value in 2.5% gelatin was higher compared to the perfusion value in both 4.5% (p = 0.009) and 6.5% gelatin (p <0.001). However, there was no significant difference in perfusion value for 4.5% and 6.5% gelatin (p = 0.051). The effect of insertion speed on the steady state perfusion value can be seen in Fig. 3f. In all of the phantoms, Fig. 3f shows that the higher the insertion speed, the higher the perfusion value.

Fig. 4a shows an example of the force and perfusion values during soft-hard transition and Fig. 4b shows an example of the force and perfusion value during hard-soft transition. The tissue transition can easily be seen from both the force and perfusion measurements in the figures. However, in the perfusion value measurement, the tissue loading stage can also easily be seen (before the rupture) for both the first and the second rupture. This implies that different tissue structures can be observed using LDF perfusion measurements.

The results of *ex-vivo* insertions can be seen in Fig. 5. For each tissue layer rupture, an increase in perfusion value can be seen. However, unlike in the tissue phantom insertions, the tissue loading stage cannot clearly be seen. These results show that LDF is a feasible method to detect tissue boundaries even in heterogeneous biological tissue.

The feasibility of an automatic puncture detection algorithm was also investigated. To do automatic puncture detection, the perfusion values were first filtered using a zero-phase low-pass filter. The local peak values were then determined where the first derivative of the filtered signals had a zero value. During the tissue puncture, the perfusion values gave a very sharp peak instead of a plateau. Therefore, the slope of the first derivative was checked where it crosses the zero value. If the slope was higher than a chosen threshold value, the points were determined as an instance of puncture. Fig. 6 shows the results of the puncture detection algorithm. The sensitivity of this method is 85%.

IV. Discussion

This work is believed to be the first investigation into steady state perfusion value as a function of tissue stiffness and into using LDF as a method to define tissue boundaries. The results presented in Section II show that it is possible to change the optical properties of the tissue phantom without affecting the modulus of elasticity of the phantom.

As can be seen in figure 3a, the tissue loading, rupture, and cutting process can easily be discerned in one-layer tissue phantoms. During tissue loading, a steady state perfusion value is observed. The perfusion value during this stage, however, is lower compared to the steady state perfusion value during the cutting process. The reason for this is due to different types of tissue deformation during these two processes. During tissue loading, the deformation is mainly in the z axis and the surface of the tissue moves together with the needle tip. This type of deformation results in a small relative velocity between the probe and the tissue in front of it. During tissue cutting, the crack extends and the tissue around the tip of the needle is pushed away into the radial direction as well [26], [27]. This process generates a higher relative velocity between the probe and the tissue compared to the tissue loading stage. Therefore,

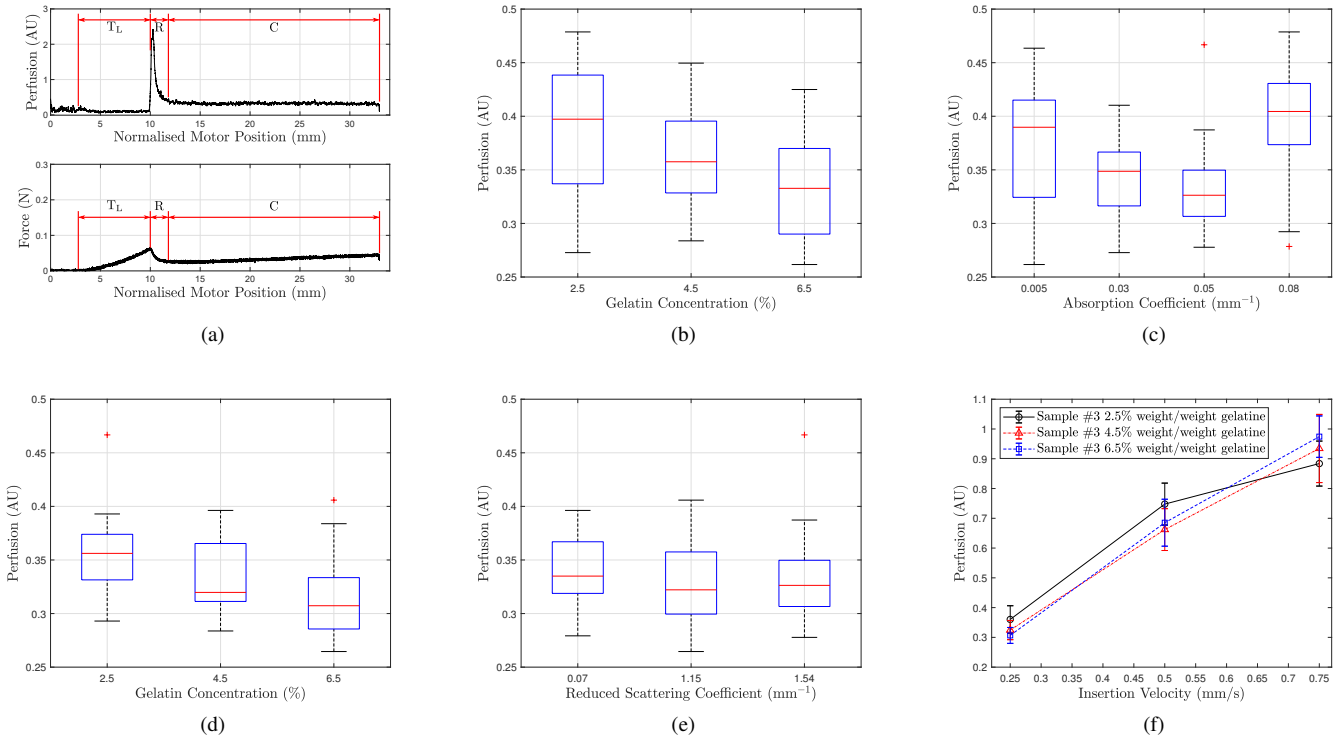

Fig. 3. a) Force and its corresponding perfusion value during needle insertion in phantom #3 with 2.5% w/w gelatin during tissue loading (T_L), rupture (R), and cutting stage (C). b) Steady state perfusion value during cutting stage of gelatin phantom with different μ_a but the same μ_s' values as a function of gelatin concentration. c) Steady state perfusion value during cutting stage of gelatin phantom as a function of μ_a. d) Steady state perfusion value during cutting stage of gelatin phantom with different μ_s' but the same μ_a values as a function of gelatin concentration. e) Steady state perfusion value during cutting stage of gelatin phantom as a function of μ_s'. f)The effect of insertion velocity on the steady state perfusion value in phantom #3

the perfusion value during the cutting stage is higher compared to the loading stage.

In the rupture process, the tissue relaxes. This process generates a high velocity in the tissue, which in turn results in a high perfusion value. During the cutting process, the LDF system combined with a controlled insertion speed gives a steady state perfusion value, regardless of the phantom's optical and mechanical properties. One of the aims of this study was to emulate the work in [6], in which it was shown that stiffer tissue has less strain compared to softer tissue. However, even though there is a statistically significant difference between different tissue stiffnesses and the steady state perfusion value, it was found that the sensitivity of the method using the steady state perfusion value in this study was not high enough to be useful (0.052 perfusion value that corresponds to 11 kPa difference in modulus elasticity).

Fig. 3f shows the effect of insertion speed in tissue phantoms with $\mu_s' = 0.77$ mm^{-1} and $\mu_a = 0.05$ mm^{-1} for three gelatin concentrations: 2.5%, 4.5% and 6.5%. The perfusion value of an LDF monitor is a function of the concentration of scattering particles and the mean velocity of moving particles [28]. The perfusion varies linearly with the particles' mean velocity but has a nonlinear relationship with the concentration of scattering particles. For a given set of optical properties, the measurement volume of the LDF probe will be the same [29]. During needle insertion, tissue deformation in front of a needle tip is a function of its stiffness where a stiffer tissue has a lower tissue deformation [14]. Due to the viscoelasticity characteristics of gelatin, the increase in the average relative velocity between the tissue and the probe may not be the same across gelatin concentrations. Therefore, the increase in perfusion value is not the same. To get a better understanding of the relationship between needle insertion speed and tissue stiffness, the tissue deformation in front of the needle tip would need to be modelled with a finite element analysis and the light transport in the tissue through Monte-Carlo simulation. This has been included in future work.

Changes in optical properties affect the penetration depth of light into tissues [29]. Therefore we believe that tissue optical properties affect the perfusion values. The increase in the absorption coefficient will reduce the detection volume of the LDF probe [29], meaning a reduction in the concentration of the moving particles. Therefore, it was hypothesised that the higher the absorption coefficient, the lower the perfusion values, which was the case in $\mu_a = 0.003 - 0.05$ mm^{-1}. Even though the detection volume was lower, the average relative velocity of the moving particles may have been higher for $\mu_a = 0.08$ mm^{-1}, due to the probe only detecting the high deforming tissue close to the needle tip, making the perfusion values for $\mu_a = 0.08$ mm^{-1} higher as well.

In section III-B tissue boundaries were detected based on the rupture process of the next tissue layer. It was shown that the method works for both hard-soft and soft-hard transitions, and that the tissue loading stage could easily be observed in

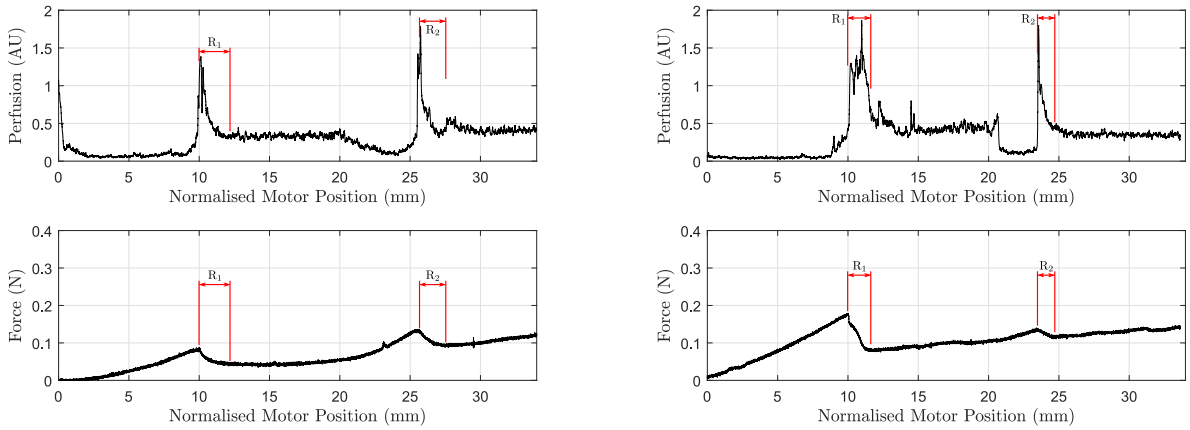

Fig. 4. a) Force and perfusion value during soft-hard phantom transition; b) force and perfusion value during hard-soft phantom transition. R_1 is the rupture of the first layer, R_2 is the rupture of the second layer

the perfusion values. This was due to the change from cutting mode into the tissue loading mode of the next layer. The advantage of tissue boundary detection based on tissue rupture is that different tissue layers could be detected as soon as the puncture happened instead of waiting to get to a steady state perfusion value.

In *ex-vivo* tissue, puncture detection can be challenging due to the tissue being heterogeneous both in terms of mechanical and optical properties. Using a tissue phantom allows homogeneous tissue properties to be created, meaning puncture can be easily shown. Despite this, punctures can still be observed in the LDF measurements with *ex-vivo* tissue. The force profile of the needle tissue insertion was similar to the force profile of the needle insertion into other tissue [30], therefore it is believed that it would work for other tissues as well. In addition, the insertion stages were also observed for other types of needle tip [31], meaning that this tissue boundary detection method could be applied to other types of needle without substantial modifications.

Using this boundary detection method, information on the actual stiffness of the tissue being traversed could not be inferred directly, but it was possible to see that a tissue boundary was being crossed, information that can be used by robots/surgeons to improve needle insertion control. Since the method can be performed in real-time, it can then be combined with another type of more precise spectroscopy system which, however, requires a longer time to collect the data, such as a Raman spectrometer system (requires 3s for one point measurement), to detect the type of tissue traversed (e.g. healthy or unhealthy tissue) [32]. Also, during percutaneous insertions into the brain, such as biopsy procedures, the insertion depth is usually defined during preoperative planning. However, due to brain shift, the position of the target can change. Since unhealthy tissue may change its tissue structure [5], whether the needle has traversed into the boundary of the target area can be checked after inserting the needle close to the planned depth.

Even though the puncture detection algorithm has been developed based on the first and second derivative of filtered perfusion values, the sensitivity of this method can still be improved. The filtering method implemented was based on a zero-phase low-pass filter. This method, however, cannot be performed in real-time. Therefore, in future works, a real-time and more sophisticated algorithm, such as an algorithm based on machine learning, will be used to determine the instance of puncture.

When a sample with a very high μ_s' (e.g. the white matter phantom) was used, a very high total light intensity (TLI) was observed, which meant the measurement was saturated. However, this was a limitation of the LDF monitor rather than the method, since it was not specifically designed for measuring deep tissue perfusion inside the brain.

In this work, the experiments were performed using a rigid needle so that the force and the perfusion values could easily be compared. Since it was shown that tissue puncture can be detected using LDF perfusion values, this method will now be implemented into the programmable bevel-tip needle (PBN). A relative offset between segments is required to steer the PBN, meaning it is not possible to ascertain which of the tip segments will detect tissue puncture first. To tackle this problem, a sensor will be embedded in each segment. Also, to ascertain that the perfusion values can still detect tissue boundaries while the needle is following a curvilinear trajectory, the perfusion values will be compared with a real-time *in-situ* imaging modality (e.g. ultrasound).

Using the LDF system to detect tissue boundaries has the following advantages: 1) Minimal changes into the needle design are needed, since the sensor can be embedded directly into the needle working channel. 2) Relatively cheap method compared to an Optical Coherence Tomography (OCT) system [33] ($7,000 for an LDF monitor compared to $40,000 for an OCT system). 3) Useful for flexible needles, whereas putting a force sensor at the base of the needle may not be feasible to measure the force at the tip (such as for a very long bevel-tip

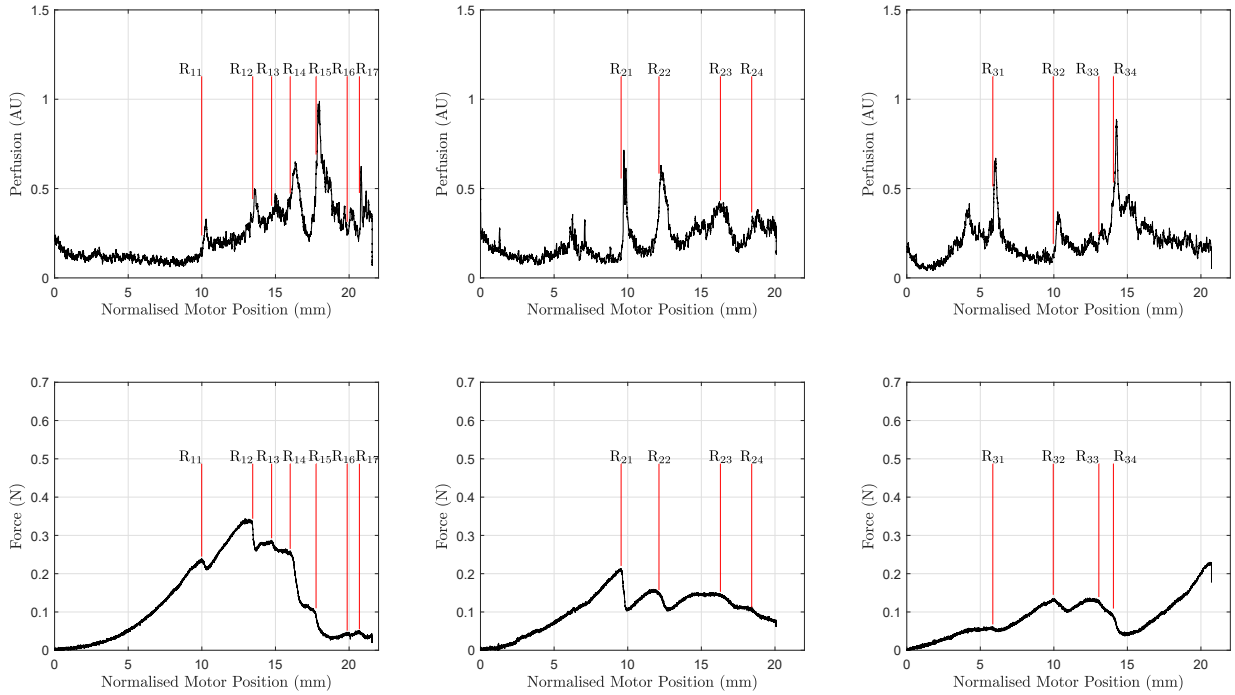

Fig. 5. Comparison between force and perfusion value measurements during *ex-vivo* insertion into a sheep's brain. In each insertion, R_{ij} shows the position where tissue rupture happened (i = insertion number, and j = rupture number)

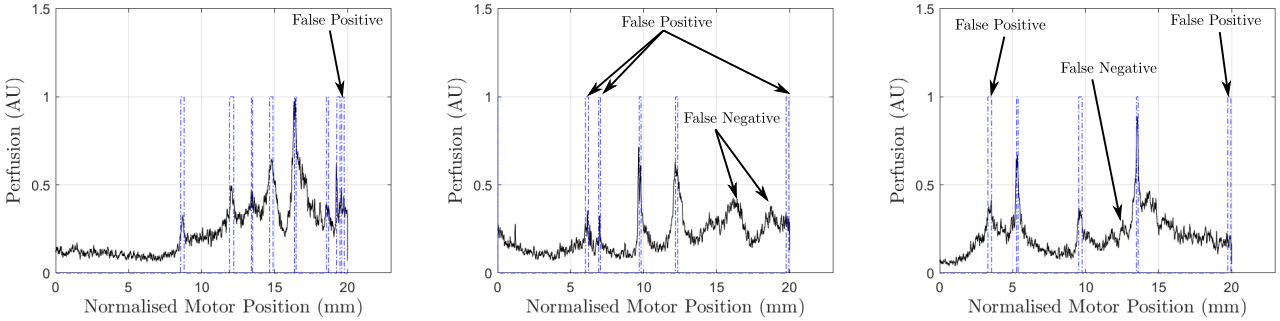

Fig. 6. The blue lines show the instances of punctures detected using the automatic detection method. The perfusion signals are the same as the perfusion signals in Fig. 5

needle combined with a broncoschope [34] and PBNs). 4) Can be used to detect both tissue boundaries and blood vessels [15], [35]. However, the measurement is limited by being noisy, and requires filtering to create an automatic detection method.

V. Conclusion and Future Work

In this paper, we show that a Laser Doppler Flowmetry (LDF) sensor at the tip of a needle can be used to detect different tissue layers. A steady-state perfusion value during tissue cutting can be used to indicate tissue stiffness, with a stiffer tissue giving a lower perfusion value. However, the sensitivity of this method is not high enough to be useful (0.05 perfusion value difference for 11 kPa difference in tissue modulus of elasticity). Tissue boundaries can be detected by observing peaked perfusion value due to tissue relaxation during tissue rupture process, which works both in a multi-layer tissue phantom and in *ex-vivo* sheep's brain. We believe that this tissue boundary detection method can be applied to other tissues and other types of needle tips since tissue puncture does not only happen during needle insertion into the brain. In future work, the finite element method (FEM) and Monte-Carlo method will be combined to determine tissue deformation/velocity in front of the probe, and simulate LDF measurements, respectively. By combining FEM and light transport simulation, a more detailed relationship between the tissue stiffness, tissue optical properties, and LDF probe geometry will be obtained. In our previous work, LDF was

used to detect deep blood vessels approaching the needle tip during insertion [15]. An approaching blood vessel will increase the perfusion values as well. Therefore a signal processing method to differentiate between tissue puncture and blood vessel detection will be developed.

ACKNOWLEDGMENTS

The authors are grateful to Oxford Optronix Ltd for the loan of the equipment and advice relating to its use.

REFERENCES

[1] M. R. Proctor and P. M. Black, *Minimally invasive neurosurgery*. Springer, 2005.

[2] E. Westebring-Van Der Putten, R. Goossens, J. Jakimowicz, and J. Dankelman, "Haptics in minimally invasive surgery–a review," *Minimally Invasive Therapy & Allied Technologies*, vol. 17, no. 1, pp. 3–16, 2008.

[3] J. F. Greenleaf, M. Fatemi, and M. Insana, "Selected methods for imaging elastic properties of biological tissues," *Annual review of biomedical engineering*, vol. 5, no. 1, pp. 57–78, 2003.

[4] S. Budday, R. Nay, R. de Rooij, P. Steinmann, T. Wyrobek, T. C. Ovaert, and E. Kuhl, "Mechanical properties of gray and white matter brain tissue by indentation," *Journal of the mechanical behavior of biomedical materials*, vol. 46, pp. 318–330, 2015.

[5] D. C. Stewart, A. Rubiano, K. Dyson, and C. S. Simmons, "Mechanical characterization of human brain tumors from patients and comparison to potential surgical phantoms," *PloS one*, vol. 12, no. 6, p. e0177561, 2017.

[6] K. M. Kennedy, B. F. Kennedy, R. A. McLaughlin, and D. D. Sampson, "Needle optical coherence elastography for tissue boundary detection," *Optics letters*, vol. 37, no. 12, pp. 2310–2312, 2012.

[7] K. M. Kennedy, R. A. McLaughlin, B. F. Kennedy, A. Tien, B. Latham, C. M. Saunders, and D. D. Sampson, "Needle optical coherence elastography for the measurement of microscale mechanical contrast deep within human breast tissues," *Journal of biomedical optics*, vol. 18, no. 12, p. 121510, 2013.

[8] N. J. van de Berg, D. J. van Gerwen, J. Dankelman, and J. J. van den Dobbelsteen, "Design choices in needle steeringa review," *IEEE/ASME Transactions on Mechatronics*, vol. 20, no. 5, pp. 2172–2183, 2014.

[9] A. Majewicz, J. J. Siegel, A. A. Stanley, and A. M. Okamura, "Design and evaluation of duty-cycling steering algorithms for robotically-driven steerable needles," in *Robotics and Automation (ICRA), 2014 IEEE International Conference on*. IEEE, 2014, pp. 5883–5888.

[10] S. Y. Ko, L. Frasson, and F. R. y Baena, "Closed-loop planar motion control of a steerable probe with a programmable bevel inspired by nature," *IEEE Transactions on Robotics*, vol. 27, no. 5, pp. 970–983, 2011.

[11] H. Kataoka, T. Washio, K. Chinzei, K. Mizuhara, C. Simone, and A. M. Okamura, "Measurement of the tip and friction force acting on a needle during penetration," in *International conference on medical image computing and computer-assisted intervention*. Springer, 2002, pp. 216–223.

[12] T. Washio and K. Chinzei, "Needle force sensor, robust and sensitive detection of the instant of needle puncture," in *International Conference on Medical Image Computing and Computer-Assisted Intervention*. Springer, 2004, pp. 113–120.

[13] S. Elayaperumal, J. H. Bae, B. L. Daniel, and M. R. Cutkosky, "Detection of membrane puncture with haptic feedback using a tip-force sensing needle," in *2014 IEEE/RSJ International Conference on Intelligent Robots and Systems*. IEEE, 2014, pp. 3975–3981.

[14] Z. Neubach and M. Shoham, "Ultrasound-guided robot for flexible needle steering," *IEEE Transactions on Biomedical Engineering*, vol. 57, no. 4, pp. 799–805, 2009.

[15] V. Virdyawan and F. R. y. Baena, "A long short-term memory network for vessel reconstruction based on laser doppler flowmetry via a steerable needle," *IEEE Sensors Journal*, pp. 1–1, 2019.

[16] L. Frasson, F. Ferroni, S. Y. Ko, G. Dogangil, and F. R. y Baena, "Experimental evaluation of a novel steerable probe with a programmable bevel tip inspired by nature," *Journal of robotic surgery*, vol. 6, no. 3, pp. 189–197, 2012.

[17] P. Å. Öberg, "Tissue motion - a disturbance in the laser-Doppler blood flow signal?" *Technol. Health Care*, vol. 7, no. 2-3, pp. 185–92, 1999.

[18] V. Virdyawan and F. R. Y. Baena, "Vessel pose estimation for obstacle avoidance in needle steering surgery using multiple forward looking sensors," in *2018 IEEE/RSJ International Conference on Intelligent Robots and Systems (IROS)*. IEEE, 2018, pp. 3845–3852.

[19] B. W. Pogue and M. S. Patterson, "Review of tissue simulating phantoms for optical spectroscopy, imaging and dosimetry," *Journal of biomedical optics*, vol. 11, no. 4, p. 041102, 2006.

[20] A. Leibinger, A. E. Forte, Z. Tan, M. J. Oldfield, F. Beyrau, D. Dini, and F. R. y Baena, "Soft tissue phantoms for realistic needle insertion: a comparative study," *Annals of biomedical engineering*, vol. 44, no. 8, pp. 2442–2452, 2016.

[21] H. G. Akarçay, S. Preisser, M. Frenz, and J. Rička, "Determining the optical properties of a gelatin-tio 2 phantom at 780 nm," *Biomedical optics express*, vol. 3, no. 3, pp. 418–434, 2012.

[22] J. R. Cook, R. R. Bouchard, and S. Y. Emelianov, "Tissue-mimicking phantoms for photoacoustic and ultrasonic imaging," *Biomedical optics express*, vol. 2, no. 11, pp. 3193–3206, 2011.

[23] A. Yaroslavsky, P. Schulze, I. Yaroslavsky, R. Schober, F. Ulrich, and H. Schwarzmaier, "Optical properties of selected native and coagulated human brain tissues in vitro in the visible and near infrared spectral range," *Physics in Medicine & Biology*, vol. 47, no. 12, p. 2059, 2002.

[24] E. Matheson, T. Watts, R. Secoli, and F. R. y Baena, "Cyclic motion control for programmable bevel-tip needle 3d steering: A simulation study," in *2018 IEEE International Conference on Robotics and Biomimetics (ROBIO)*. IEEE, 2018, pp. 444–449.

[25] D. K. Binder, G. M. Rau, and P. A. Starr, "Risk factors for hemorrhage during microelectrode-guided deep brain stimulator implantation for movement disorders," *Neurosurgery*, vol. 56, no. 4, pp. 722–732, 2005.

[26] M. Mahvash and P. E. Dupont, "Mechanics of dynamic needle insertion into a biological material," *IEEE Transactions on Biomedical Engineering*, vol. 57, no. 4, pp. 934–943, April 2010.

[27] M. Oldfield, D. Dini, G. Giordano, and F. Rodriguez y Baena, "Detailed finite element modelling of deep needle insertions into a soft tissue phantom using a cohesive approach," *Computer methods in biomechanics and biomedical engineering*, vol. 16, no. 5, pp. 530–543, 2013.

[28] I. Fredriksson, C. Fors, and J. Johansson, "Laser doppler flowmetry-a theoretical framework," *Department of Biomedical Engineering, Linköping University*, pp. 6–7, 2007.

[29] I. Fredriksson *et al.*, "Measurement depth and volume in laser Doppler flowmetry," *Microvasc. Res.*, vol. 78, no. 1, pp. 4–13, 2009.

[30] N. Abolhassani, R. Patel, and M. Moallem, "Needle insertion into soft tissue: A survey," *Medical engineering & physics*, vol. 29, no. 4, pp. 413–431, 2007.

[31] S. Jiang, P. Li, Y. Yu, J. Liu, and Z. Yang, "Experimental study of needle–tissue interaction forces: effect of needle geometries, insertion methods and tissue characteristics," *Journal of biomechanics*, vol. 47, no. 13, pp. 3344–3353, 2014.

[32] J. Desroches, M. Jermyn, M. Pinto, F. Picot, M.-A. Tremblay, S. Obaid, E. Marple, K. Urmey, D. Trudel, G. Soulez, *et al.*, "A new method using raman spectroscopy for in vivo targeted brain cancer tissue biopsy," *Scientific reports*, vol. 8, no. 1, p. 1792, 2018.

[33] C. P. Liang *et al.*, "Coherence-gated Doppler: a fiber sensor for precise localization of blood flow." *Biomed. Opt. Express*, vol. 4, no. 5, pp. 760–71, 2013.

[34] P. J. Swaney, A. W. Mahoney, B. I. Hartley, A. A. Remirez, E. Lamers, R. H. Feins, R. Alterovitz, and R. J. Webster III, "Toward transoral peripheral lung access: Combining continuum robots and steerable needles," *Journal of medical robotics research*, vol. 2, no. 01, p. 1750001, 2017.

[35] K. Wardell *et al.*, "High-Resolution Laser Doppler Measurements of Microcirculation in the Deep Brain Structures: A Method for Potential Vessel Tracking," *Stereotact. Funct. Neurosurg.*, pp. 1–9, 2016.